Eur. Phys. J. B **10**, 515–523 (1999)

THE EUROPEAN PHYSICAL JOURNAL B

EDP Sciences

Water droplets in a spherically confined nematic solvent: A numerical investigation

H. Stark[1,a], J. Stelzer[1], and R. Bernhard[2]

[1] Institut für Theoretische und Angewandte Physik, Universität Stuttgart, Pfaffenwaldring 57, 70550 Stuttgart, Germany
[2] IMPACT Meßtechnik GmbH, Maybachstr. 25, 71332 Waiblingen, Germany

Received 11 December 1998

Abstract. Recently, it was observed that water droplets suspended in a nematic liquid crystal form linear chains [Poulin *et al.*, Science **275**, 1770 (1997)]. The chaining occurs, *e.g.*, in a large nematic drop with homeotropic boundary conditions at all the surfaces. Between each pair of water droplets a point defect in the liquid crystalline order was found in accordance with topological constraints. This point defect causes a repulsion between the water droplets. In our numerical investigation we limit ourselves to a chain of two droplets. For such a complex geometry we use the method of finite elements to minimize the Frank free energy. We confirm an experimental observation that the distance d of the point defect from the surface of a water droplet scales with the radius r of the droplet like $d \approx 0.3r$. When the water droplets are moved apart, we find that the point defect does not stay in the middle between the droplets, but rather forms a dipole with one of them. This confirms a theoretical model for the chaining. Analogies to a second order phase transition are drawn. We also find the dipole when one water droplet is suspended in a bipolar nematic drop with two boojums, *i.e.*, surface defects at the outer boundary. Finally, we present a configuration where two droplets repel each other without a defect between them.

PACS. 77.84.Nh Liquids, emulsions, and suspensions; liquid crystals – 61.30.Cz Theory and models of liquid crystal structure – 61.30.Jf Defects in liquid crystals

1 Introduction

Liquid crystal research is, without any doubt, strongly driven by its importance for technological applications, namely display devices. On the other hand, topological point and line defects in the liquid crystalline order, which occur as a consequence of the broken rotational symmetry of the isotropic space [1–5], attract a lot of attention since they are fascinating by themselves. They, furthermore, influence the static and dynamic properties of the system under investigation. Conventional displays, like twisted nematic [6] or surface-stabilized ferroelectric liquid crystal cells [7], possess a simple geometry, where the liquid crystal is enclosed between two parallel glass plates. With the introduction of polymer-dispersed liquid crystals as electrically controllable light shutters [8,9], an extensive study of liquid crystals confined to complex geometries, like drops in a polymer matrix or a random porous network in silica aerogel, was initiated [9,10].

This article presents a numerical investigation of the interesting inverse problem, which is posed by particles suspended in a nematic solvent. In a nematic liquid crystal the molecules align on average along a unit vector $\mathbf{n}$, called director. The energetic ground state is a uniform director field throughout space. Due to the anchoring of the molecules at the surface of a particle the surrounding director field is elastically distorted. In addition to conventional van der Waals forces, screened Coulomb and steric interactions [11], the elastic deformation of the director field mediates a further interaction between the particles. Point defects give rise to a short-range repulsion.

Already in 1970, Brochard and de Gennes studied a suspension of magnetic grains in a nematic liquid crystal and determined the director field far away from a particle [12]. Chaining of bubbles or microcrystallites was used to visualize the director field close to the surface of liquid crystals [13,14]. A bistable liquid crystal display was introduced based on a dispersion of agglomerations of silica spheres in a nematic host [15–17]. Chains and clusters were observed in the dispersion of latex particles in a lyotropic liquid crystal [18–20]. The radii of the particles were 60 and 120 nm. Therefore, details of the director field could not be resolved under the polarizing microscope. Terentjev *et al.* investigated the director field around a sphere by both analytical and numerical methods [21–23]. For homeotropic boundary conditions of the director, they considered the Saturn-ring configuration where the sphere is surrounded by a $-1/2$ disclination ring. The long-range quadrupolar interaction of such objects was determined by Ramaswamy *et al.* [24] and Ruhwandl and Terentjev [25].

[a] e-mail: holger@itap.physik.uni-stuttgart.de

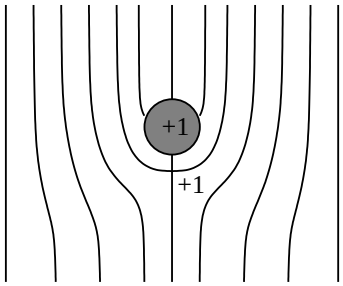

Fig. 1. The water droplet and its companion hyperbolic hedgehog form a dipole. Both the droplet and the hedgehog carry a topological charge +1, and the total charge of the dipole is $0 = |1 - 1|$.

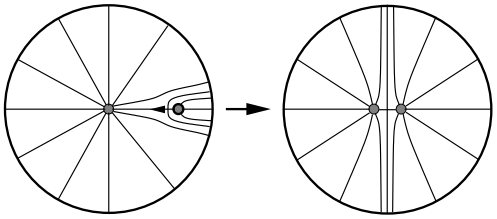

Fig. 2. Scenario to explain the chaining of water droplets in a large nematic drop. The right water droplet and its companion hyperbolic hedgehog form a dipole, which is attracted by the strong splay deformation around the droplet in the center (left picture). The dipole moves towards the center until at short distances the repulsion mediated by the point defect sets in (right picture).

Even two parallel plates, immersed into the isotropic phase close to the isotropic-nematic phase transition, interact as a result of a surface-induced nematic order [26].

1.1 Inverted nematic emulsions

The present article addresses recent work on inverted nematic emulsions where surfactant-coated water droplets are dispersed in a nematic solvent [27,28]. The advantage of such a system is that the particles are easily observable by polarizing microscopy since the size of the water droplets is of the order of a micron. Furthermore, the anchoring of the liquid crystal molecules on the surfaces of the droplets are controllable *via* the surfactant. Understanding the suspension of such large particles will, without any doubt, help to clarify the observations of dispersions of smaller objects. The most striking feature, from a theoretical point of view, is that inverted emulsions provide an ideal laboratory for the investigation of topological defects. In inverted emulsions point defects, also called hedgehogs, occur. They carry a topological charge q specifying the number of times the unit sphere is wrapped by the director $\mathbf{n}$ on any surface enclosing the defect core. Since all properties of the nematic phase are invariant under the inversion $\mathbf{n} \to -\mathbf{n}$, q is always positive, and two hedgehogs with respective charges q_1 and q_2 "add up" to a total topological charge of either $q_1 + q_2$ or $|q_1 - q_2|$ [4].

When a water droplet with homeotropic, *i.e.*, perpendicular anchoring of the director at its surface is placed into a uniformly aligned nematic liquid crystal, a hyperbolic hedgehog is nucleated (see Fig. 1). The droplet and its tightly bound companion defect provide a key unit to understand inverted nematic emulsions [27–30]. We will call it a dipole for short because of its dipolar symmetry. Both the water droplet and the hyperbolic hedgehog carry a topological charge +1 which "add up" to the total charge 0 of the dipole. A phenomenological theory predicts that the dipole couples to a strong splay deformation in the director field [27,30]. Two parallel dipoles are attracted *via* a long-range dipolar interaction which explains the observed chaining of water droplets [27,28,30]. A quantitative confirmation of the dipolar interaction was presented recently [31].

In our numerical investigation we consider multiple nematic emulsions where the nematic host fluid containing the water droplets is confined to large nematic drops, which, in turn, are surrounded by water. The water droplets also form chains with a hyperbolic hedgehog situated between two droplets (see Fig. 2, right) [27,28]. In the experiment it was found that the distance d of the point defect from the surface of a water droplet scales with the radius r of the droplet like $d \approx 0.3r$ [27,28]. In the following we will call this relation the scaling law. A possible explanation for the chaining, as in a uniformly aligned sample, could be the presence of a dipole. One water droplet fits perfectly into the center of a large nematic drop, which has a total topological charge +1. Any additional water droplet has to be accompanied by a hyperbolic hedgehog in order not to change the total charge. If the dipole forms (see Fig. 2, left), it is attracted by the strong splay deformation in the center [30], until a short-range repulsion mediated by the defect sets in [27,28].

1.2 Main results

By our numerical investigations we confirm the scaling law, for which we find $d = (0.325 \pm 0.025)\, r$, and discuss the influence of the outer boundary of the large drop. We, furthermore, show that in nematic drops the dipole also exists, confirming the scenario of Figure 2. When the two water droplets in the right picture of Figure 2 are moved apart symmetrically about the center of the large drop, the dipole forms *via* a second order phase transition. We also identify the dipole in a bipolar configuration which occurs for planar boundary conditions at the outer surface of the nematic drop. Two boojums, *i.e.*, surface defects appear [32–34], and the dipole is attracted by the strong splay deformation in the vicinty of one of them [27,28,30]. Besides the dipole we find another stable configuration in this geometry, where the hyperbolic hedgehog sits close to one of the boojums. Finally, we show that water droplets can repel each other without a hyperbolic defect placed between them.

To minimize the Oseen-Zöcher-Frank free energy [36] for different positions of the water droplets, we employ the method of finite elements [35], which is most suitable

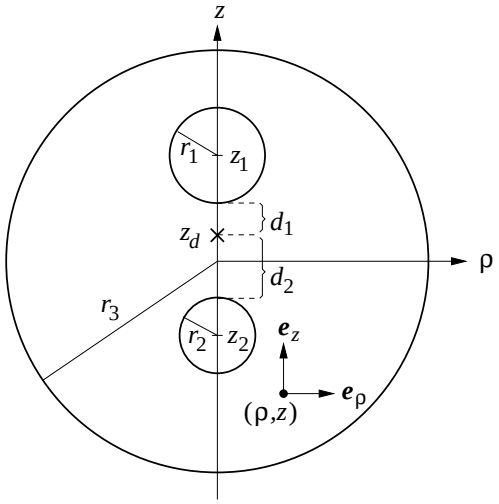

Fig. 3. Geometry parameters for two water droplets with respective radii r_1 and r_2 in a large nematic drop with radius r_3. The system is axially symmetric about the z axis, and cylindrical coordinates ρ, z are used. The coordinates z_1, z_2, and z_d are the respective positions of the two droplets and the hyperbolic hedgehog. The two distances of the hedgehog from the surfaces of the droplets are d_1 and d_2.

for non-trivial geometries. For the interested reader we provide a more detailed description of it in Section 2 and in the Appendix. We hope to stimulate further applications of the method of finite elements to liquid crystals in complex geometries. Before we discuss our results in Section 3, we define the geometries and present numerical details in Section 2.

2 Geometries and numerical methods

In our article we numerically investigate two particular geometries of axial symmetry. The first problem is defined in Figure 3. We consider two spherical water droplets with respective radii r_1 and r_2 in a large nematic drop with radius r_3. The whole system possesses axial symmetry, so that the water droplets and the hyperbolic hedgehog, indicated by a cross, are located always on the z axis. We employ a cylindrical coordinate system. The coordinates z_1, z_2, and z_d denote, respectively, the positions of the centers of the droplets and of the hyperbolic hedgehog on the z axis. The distances of the hedgehog from the surfaces of the two water droplets are, respectively, d_1 and d_2. Then, the quantity $d_1 + d_2$ means the distance of the two small spheres, and the point defect is situated in the middle between them if $d_1 = d_2$. We, furthermore, restrict the nematic director to the (ρ, z) plane, which means that we do not allow for twist deformations [37]. The director is expressed in the local coordinate basis $(\mathbf{e}_\rho, \mathbf{e}_z)$ of the cylindrical coordinate system,

$$\mathbf{n}(\rho, z) = \sin\Theta(\rho, z)\mathbf{e}_\rho + \cos\Theta(\rho, z)\mathbf{e}_z, \tag{1}$$

where we introduced the *tilt angle* Θ. It is always restricted to the range $[-\pi/2, \pi/2]$ to ensure the $\mathbf{n} \to -\mathbf{n}$ symmetry of the nematic phase. At all the boundaries we assume a rigid homeotropic anchoring of the director, which allows us to omit any surface term in the free energy. In reference [30] it was shown that rigid anchoring is justified in our system and that any deformation of the water droplets can be neglected.

In the second problem we have only one water droplet inside a large nematic drop. We use the same coordinates and lengths as described in Figure 3, but omit the second droplet. The anchoring of the director at the outer surface of the large nematic sphere is rigid planar. At the surface of the small sphere we again choose a homeotropic boundary condition.

We write the Oseen-Zöcher-Frank free energy density [36] for the director field (1) in units of K_{33}/a^2, where K_{33} is the bend elastic constant and a the characteristic length scale of our system, typically several microns:

$$\begin{aligned}\overline{f}(\Theta) &= \frac{f(\Theta)}{K_{33}/a^2} \\ &= \frac{\overline{K}_{11}}{2}\left(\frac{\sin\Theta}{\rho} + \Theta_\rho\cos\Theta - \Theta_z\sin\Theta\right)^2 \\ &\quad + \frac{1}{2}\left(\Theta_z\cos\Theta + \Theta_\rho\sin\Theta\right)^2. \end{aligned}\tag{2}$$

All lengths are given relative to a, and $\overline{K}_{11} = K_{11}/K_{33}$ is the scaled splay constant. The indices ρ and z indicate, respectively, partial derivatives $\partial/\partial\rho$ and $\partial/\partial z$.

In order to find the equilibrium director field, the reduced free energy in units of $K_{33}a$,

$$\overline{F} = \int \mathrm{d}^3x\,\overline{f}(\Theta), \tag{3}$$

is minimized on a grid. Because of the nontrivial geometry of our problem, we decided to employ the method of finite elements [35], where the integration area is covered with triangles. We note that for simpler geometries the method of finite differences is usually used, where the grid is defined by the coordinate lines. We construct a net of triangles by covering our integration area with a hexagonal lattice with lattice constant b. Vertices of triangles that only partially belong to the integration area are moved onto the boundary along the radial direction of the appropriate sphere. As a result, extremely obtuse triangles occur close to the boundary. We use a relaxation mechanism to smooth out these irregularities. The final triangulation is shown in Figure 4. In the area between the small spheres, where the hyperbolic hedgehog is situated, the grid is further subdivided to account for the strong director deformations close to the point defect.

The reduced free energy $\overline{F}$ in units of $K_{33}a$ is written as a function of the tilt angles Θ_i $(i = 1, \ldots, n)$ at the n vertices of the grid: $\overline{F} = \overline{F}[\boldsymbol{\Theta}]$, where $\boldsymbol{\Theta} = (\Theta_1, \ldots, \Theta_n)$. For further explanations, how $\overline{F}[\boldsymbol{\Theta}]$ is constructed within the method of finite elements, we refer the reader to the Appendix. To find a minimum of the free energy, we start with a configuration that already possesses the hyperbolic

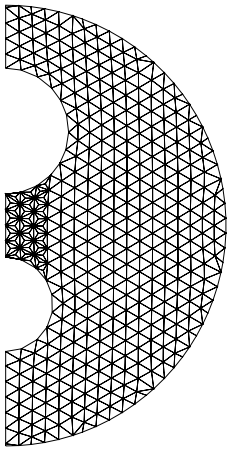

Fig. 4. Triangulation of the integration area (lattice constant: $b = 0.495$). Between the small spheres a refined net of triangles is chosen.

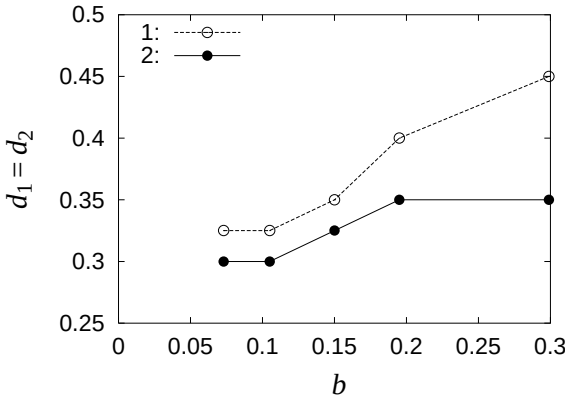

Fig. 5. The equilibrium distance $d_1 = d_2$ between the defect and the surfaces of the spheres as a function of the lattice constant b. The small spheres are placed symmetrically about $z = 0$, *i.e.*, $z_1 = -z_2$. The radii are $r_1 = r_2 = 1$. Curve 1: no grid refinement, curve 2: one step of grid refinement.

point defect at z_d and let it relax *via* the standard Newton-Gauss-Seidel method [39]:

$$\Theta_i^{\mathrm{new}} = \Theta_i^{\mathrm{old}} - \frac{\partial \overline{F}[\boldsymbol{\Theta}]}{\partial \Theta_i} \Big/ \frac{\partial^2 \overline{F}[\boldsymbol{\Theta}]}{\partial \Theta_i^2} \; . \tag{4}$$

The derivatives $\overline{F}$ with respect to Θ_i are performed numerically. Although the point defect is not fixed to its original position during the relaxation, it never moves into the global minimum, but rather stays where we place it. We use this fact to plot energy curves *versus* the position of the point defect. Other starting configurations, *e.g.*, a uniform director field throughout the integration area or randomly oriented directors on the grid, do not produce the hyperbolic hedgehog, but instead relax into a configuration with a higher energy, which we briefly investigate in Section 3.4.

Integrating the free energy density over one triangle, yields a line energy, *i.e.*, an energy per unit length. As a rough estimate for its upper limit, we introduce the line tension $f_\mathrm{l} = (\overline{K}_{11}+1)/2$ of the isotropic core of a disclination [36]. Whenever the numerically calculated local line energy is larger than f_l, we replace it by f_l. As a result, the hyperbolic point defect is stabilized against opening up to a disclination ring.

All our calculations are preformed for the nematic liquid crystal pentylcyanobiphenyl (5CB), for which the experiments were done [27,28]. It has a bend elastic constant $K_{33} = 0.53 \times 10^{-6}$ dyn and a scaled splay elastic constant $\overline{K}_{11} = K_{11}/K_{33} = 0.79$. The experimental ratio $r_3/r_{1/2}$ of the radii of the large and small drops is in the range 10–50 [27,28]. The difficulty is that we want to investigate details of the director field close to the small spheres which requires a fine triangulation on the length scale given by $r_{1/2}$. To keep the computing time to a reasonable value, we choose the following lengths: $r_3 = 7$, $r_{1/2} = 0.5 \ldots 2$, and $b = 0.195$ for the lattice constant of the grid. In addition, we normally use one step of grid refinement between the small spheres (geometry 1) or between the small sphere and the south pole of the large nematic drop (geometry 2). With such parameters we obtain a lattice with 2 200–2 500 vertices.

In order to estimate the accuracy of our numerical calculations, we performed a time-consuming series of computations for various values of the grid size without and with one step of grid refinement. As an example we chose to determine the distances d_1 and d_2 between the hyperbolic point defect and the surfaces of the water droplets that correspond to the minimum energy configuration. The parameters were $r_1 = r_2 = 1$, and the spheres 1 and 2 were placed symmetrically about the center, *i.e.*, $z_1 = -z_2$. As explained in the next section, the defect always stays in the middle between the two spheres, which means $d_1 = d_2$. The result of our analysis is presented in Figure 5 where we plot $d_1 = d_2$ *versus* the lattice constant b of our grid. As expected, the dependence of the distance $d_1 = d_2$ on the grid size is of minor importance when we apply a local refinement of the grid according to Figure 4. Furthermore, when decreasing the grid constant below 0.1 there is hardly any change in the distance. This gives us confidence that the method of finite elements is appropriate to provide quantitative and error-controlled solutions for director fields in complex geometries that even contain non-trivial topological objects. As stated above, in order to keep the computer time at a reasonable amount we generally performed our calculations at a grid constant of 0.195 with one step of grid refinement. According to our analysis in Figure 5, this corresponds to a maximum error of *ca.* 15%.

3 Results and discussion

In this section we discuss the results from our numerical investigation. We will mainly address the following questions.

1. Can we confirm the scaling law $d_{1/2} \approx 0.3\, r_{1/2}$, which was observed in experiment, by varying the different lengths in our geometry?

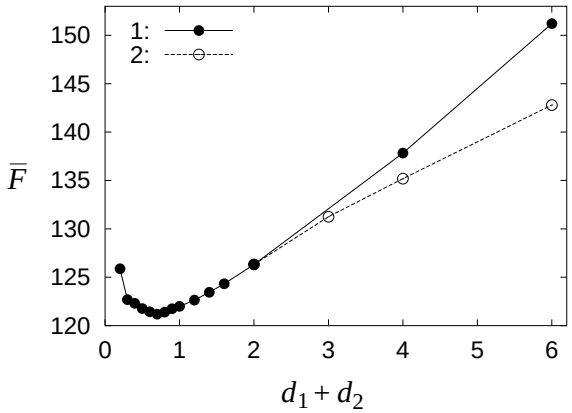

Fig. 6. The free energy $\overline{F}$ as a function of the distance $d_1 + d_2$ between the small spheres which are placed symmetrically about $z = 0$ ($r_1 = r_2 = 1$). Curve 1: $z_\mathrm{d} = 0$, curve 2: position z_d of the defect can relax along the z axis.

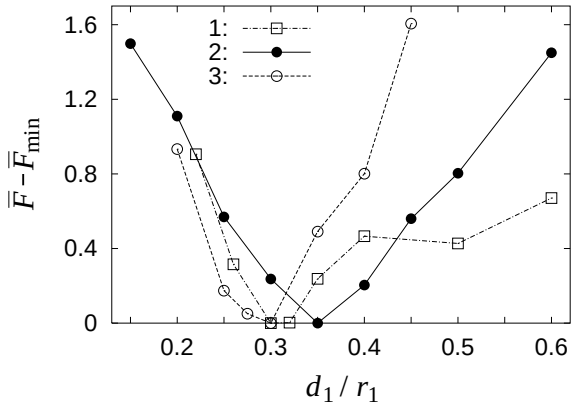

Fig. 7. The free energy $\overline{F} - \overline{F}_{\min}$ as a function of $d_1/r_1 = d_2/r_2$. The small spheres are placed symmetrically about $z = 0$. Curve 1: $r_1 = r_2 = 0.5$, curve 2: $r_1 = r_2 = 1$, and curve 3: $r_1 = r_2 = 2$.

2. Does the dipole formed by a water droplet and its companion hyperbolic defect, which is well-established for a director field uniformly aligned at infinity, also have a meaning in more complex geometries?
3. Is the hyperbolic hedgehog necessary to mediate a repulsion between the water droplets? To answer this question, we will investigate a configuration with disclination rings around the small spheres.

3.1 Scaling law

We start with the first question. In Figure 6 we plot the reduced free energy $\overline{F}$ as a function of the distance $d_1 + d_2$ between the surfaces of the small spheres, which are placed symmetrically about the center, *i.e.*, $z_2 = -z_1$. Their radii are $r_1 = r_2 = 1$. Curve 1 shows a clear minimum at $d_1 + d_2 \approx 0.7$, the defect stays in the middle between the two spheres at $z_\mathrm{d} = 0$. In curve 2 we move the defect along the z axis and plot the minimum free energy for each fixed distance $d_1 + d_2$. It is obvious that beyond $d_1 + d_2 = 2$ the defect moves to one of the small spheres. We will investigate this result in more detail in the following section.

In Figure 7 we take three different radii for the small spheres, $r_1 = r_2 = 0.5, 1, 2$, and plot the free energy *versus* d_1/r_1 close to the minimum. Recall that d_1 is the distance of the hedgehog from the surface of sphere 1. Since for such small distances $d_1 + d_2$ the defect always stays at $z_\mathrm{d} = 0$, *i.e.*, in the middle between the two spheres, we have $d_1/r_1 = d_2/r_2$. The quantity $\overline{F}_{\min}$ refers to the minimum free energy of each curve. For each of the three radii we obtain an energetically preferred distance d_1/r_1 in the range of [0.3, 0.35], which agrees well with the experimental value of 0.3. Why does a scaling law of the form $d_{1/2} = (0.325 \pm 0.025)\, r_{1/2}$ occur? If the small spheres are far away from the surface of the large nematic drop, its finite radius r_3 should hardly influence the distances d_1 and d_2. Then, the only length scale in the system is $r_1 = r_2$, and we expect $d_{1/2} \propto r_{1/2}$. However, in Figure 7 the influence from the boundary of the large sphere is already visible. Let us take curve 2 for spheres with radii $r_{1/2} = 1$ as a reference. It looks pretty symmetric around $d_1/r_1 = 0.35$. The slope of the right part of curve 3, which corresponds to larger spheres of radii $r_{1/2} = 2$, is steeper than in curve 2. Also, the location of the minimum clearly tends to values smaller than 0.3. We conclude that the small spheres are already so large that they are strongly repelled by the boundary of the nematic drop. On the other hand, the slope of the right part of curve 1, which was calculated for spheres of radii $r_{1/2} = 0.5$, is less steep than in curve 2. This leads to the conclusion that the boundary of the nematic drop has only a minor influence on such small spheres.

When we move the two spheres with radii $r_{1/2} = 1$ together in the same direction along the z axis, the defect always stays in the middle between the droplets and obeys the scaling law. We have tested its validity within the range [0, 3] for the defect position z_d. Of course, the absolute minimum of the free energy occurs in the symmetric position of the two droplets, $z_2 = -z_1$.

We further check the scaling law for $r_1 \neq r_2$. We investigate two cases. When we choose $r_1 = 2$ and $r_2 = 0.6$, we obtain $d_{1/2} \approx 0.3\, r_{1/2}$. In the second case, $r_1 = 2$ and $r_2 = 1$, we find $d_1 \approx 0.37\, r_1$ and $d_2 \approx 0.3\, r_2$. As observed in the experiment, the defect sits always closer to the smaller sphere. There is no strong deviation from the scaling law $d_{1/2} = (0.325 \pm 0.025)\, r_{1/2}$, although we would allow for it, since $r_1 \neq r_2$.

3.2 Identification of the dipole

The second question is if the dipole formed by one water droplet and a companion hyperbolic point defect has a meaning in our geometry. To answer this question, we place sphere 2 with radius $r_2 = 1$ in the center of the nematic drop at $z_2 = 0$. Then, we determine the energetically preferred position of the point defect for different locations z_1 of sphere 1 ($r_1 = 1$). The position of the hedgehog is indicated by $\Delta = (d_2 - d_1)/(d_1 + d_2)$.

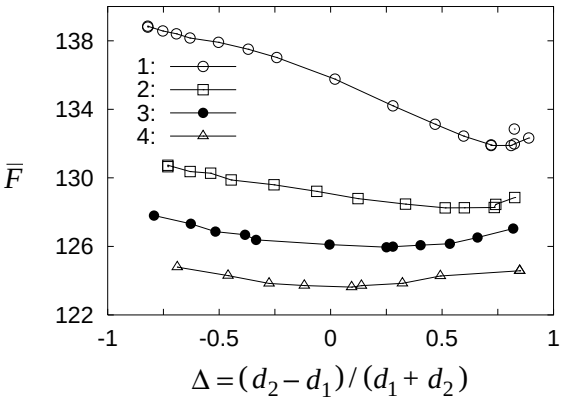

Fig. 8. The free energy $\overline{F}$ as a function of $\Delta = (d_2 - d_1)/(d_1 + d_2)$. Sphere 2 is placed at $z_2 = 0$. The position z_1 of sphere 1 is the parameter. Curve 1: $z_1 = 5$, curve 2: $z_1 = 4$, curve 3: $z_1 = 3.5$, and curve 4: $z_1 = 3$. The radii are $r_1 = r_2 = 1$.

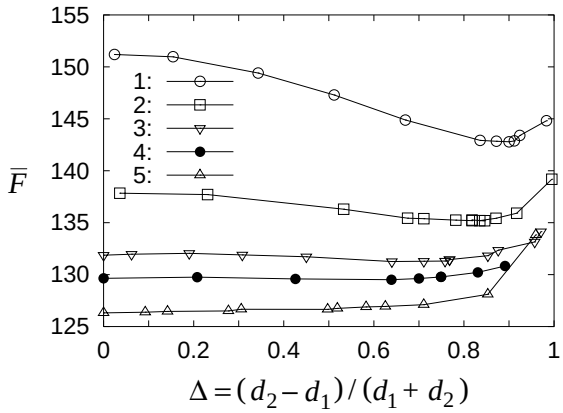

Fig. 9. The free energy $\overline{F}$ as a function of $\Delta = (d_2 - d_1)/(d_1 + d_2)$. The small spheres are placed symmetrically about $z = 0$. Curve 1: $z_1 = -z_2 = 4$, curve 2: $z_1 = -z_2 = 3$, curve 3: $z_1 = -z_2 = 2.5$, curve 4: $z_1 = -z_2 = 2.3$, curve 5: $z_1 = -z_2 = 2$. The radii are $r_1 = r_2 = 1$.

If the defect is located in the middle between the two spheres, Δ is zero since $d_1 = d_2$. On the other hand, if it sits at the surface of sphere 1, Δ is one since $d_1 = 0$. In Figure 8 we plot the free energy $\overline{F}$ *versus* Δ. In curve 1, where the small spheres are farthest apart from each other ($z_1 = 5$), we clearly find the defect close to sphere 1. This verifies that the dipole is existing. It is thermally stable, since a rough estimate of the thermally induced mean displacement of the defect yields 0.01 [30]. When sphere 1 is approaching the center (curve 2: $z_1 = 4$ and curve 3: $z_1 = 3.5$), the defect moves away from the droplets until it nearly reaches the middle between both spheres (curve 4: $z_1 = 3$). This means, the dipole vanishes gradually until the hyperbolic hedgehog is shared by both water droplets.

An interesting situation occurs when sphere 1 and 2 are placed symmetrically about $z = 0$. Then, the defect has two equivalent positions on the positive and negative part of the z axis. In Figure 9 we plot again the free energy $\overline{F}$ *versus* the position Δ of the defect. From curve 1 to 3 ($z_1 = z_2 = 4$, 3, 2.5) the minimum in $\overline{F}$ becomes broader and more shallow. The defect moves closer towards the center until at around $z_1 = -z_2 = 2.3$ (curve 4) it reaches $\Delta = 0$. This is reminiscent to a symmetry-breaking second order phase transition [5,40] which occurs when, in the course of moving the water droplets apart, the dipole starts to form. We take Δ as an order parameter, where $\Delta = 0$ and $\Delta \neq 0$ describe, respectively, the high- and the low-symmetry phase. A Landau expansion of the free energy yields

$$\overline{F}(\Delta) = \overline{F}_0(z_1) + a_0[2.3 - z_1]\Delta^2 + c(z_1)\Delta^4, \qquad (5)$$

where $z_1 = -z_2$ plays the role of the temperature. Odd powers in Δ are not allowed because of the required symmetry $\overline{F}(\Delta) = \overline{F}(-\Delta)$. This free energy qualitatively describes the curves in Figure 9. It should be possible to observe such a "second order phase transition" [41] with a method introduced recently by Poulin *et al.* [31] to measure dipolar forces in inverted nematic emulsion. When the two small droplets are filled with a magnetorheological fluid instead of pure water, a small magnetic field of about 100 G, applied perpendicular to the z axis, induces two parallel magnetic dipoles. Since they repel each other, the two droplets are forced apart. When the magnetic field is switched off, the two droplets move towards each other to reach the equilibrium distance. In the course of this process, the phase transition for the dipole should be observable.

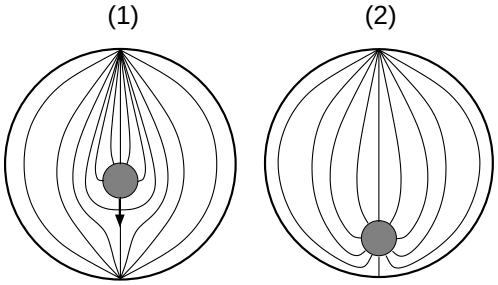

Fig. 10. Planar boundary conditions at the outer surface of the large sphere create boojums, *i.e.*, surface defects at the north and the south pole. A water droplet with homeotropic boundary conditions nucleates a hyperbolic hedgehog. Two configurations exist that are either stable or metastable depending on the position of the water droplet; (1) the dipole, (2) the hyperbolic hedgehog sitting at the surface.

3.3 The dipole in a bipolar configuration

It is possible to change the anchoring of the director at the outer surface of the large nematic drop from homeotropic to planar by adding some amount of glycerol to the surrounding water phase [27]. Then, the bipolar configuration for the director field appears [33,34], where two boojums [32], *i.e.*, surface defects of charge 1 are situated at the north and south pole of the large nematic drop (see configuration (1) in Fig. 10). The topological point charge of the interior of the nematic drop is zero, and every small water droplet with homeotropic boundary condition has

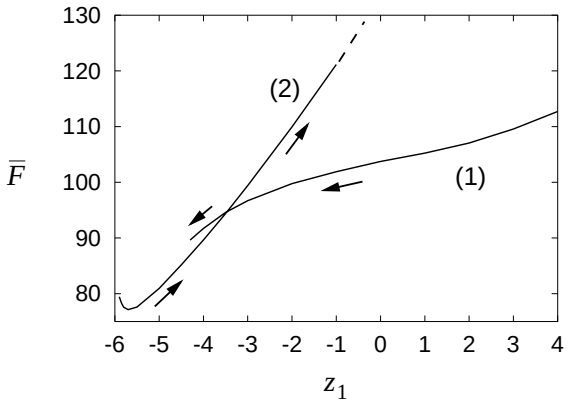

Fig. 11. The free energy $\overline{F}$ as a function of the position z_1 of the water droplet for the configurations (1) and (2). For $z_1 > -3.5$, (1) is stable, and (2) is metastable. The situation is reversed for $-4.3 < z_1 < -3.5$. Configuration (1) loses its metastability at $z_1 = -4.3$.

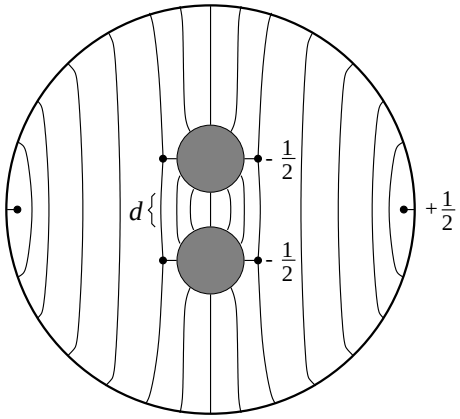

Fig. 12. An alternative metastable configuration. Both droplets are surrounded by a $-1/2$ disclination ring which compensates the topological charge $+1$ of each droplet. An additional $+1/2$ disclination ring close to the surface of the nematic drop satisfies the total topological charge $+1$.

to be accompanied by a hyperbolic hedgehog. In the experiment the hedgehog sits close to the water droplet, *i.e.*, the dipole exists and it is attracted by the strong splay deformation close to the south pole [27], as predicted by the phenomenological theory [27,30].

A numerical analysis of the free energy $\overline{F}$ is in agreement with experimental observations but also reveals some interesting details which have to be confirmed. In Figure 11 we plot $\overline{F}$ as a function of the position z_1 of the small water droplet with radius $r_1 = 1$. The diagram consists of curves (1) and (2), which correspond, respectively, to configurations (1) and (2) in Figure 10. The free energy possesses a minimum at around $z_1 = -5.7$. The director field assumes configuration (2), where the hyperbolic hedgehog is situated at the surface of the nematic drop. Moving the water droplet closer to the surface induces a repulsion due to the strong director deformations around the point defect. When the water droplet is placed far away from the south pole, *i.e.*, at large z_1, the dipole of configuration (1) forms and represents the absolute stable director field. At $z_1 = -3.5$ the dipole becomes metastable but the system does not assume configuration (2) since the energy barrier, the system has to overcome by thermal activation, is much too high. By numerically calculating the free energy for different positions of the hedgehog, we have, *e.g.*, at $z_1 = -4.0$ determined an energy barrier of $K_{33}a \approx 1000\, k_{\mathrm{B}}T$, where k_{B} is the Boltzmann constant, T the room temperature, and $a \approx 1\,\mu$m. At $z_1 = -4.3$ the dipole even loses its metastability, the hyperbolic defect jumps to the surface at the south pole, and the water droplet follows until it reaches its energetically preferred position. On the other hand, if it were possible to move the water droplet away from the south pole, the hyperbolic hedgehog would stay at the surface, since configuration (2) is always metastable for $z_1 \geq -3.5$. The energy barrier for a transition to the dipole is again at least $1000\ k_{\mathrm{B}}T$. We have also investigated the distance d_1 of the defect from the surface of the water droplet. For $z_1 \in [-2, 4]$, d_1 fluctuates between 0.3 and 0.35. For $z_1 < -2$, it increases up to 0.5 at $z_1 = -4.3$, where the dipole loses its metastability.

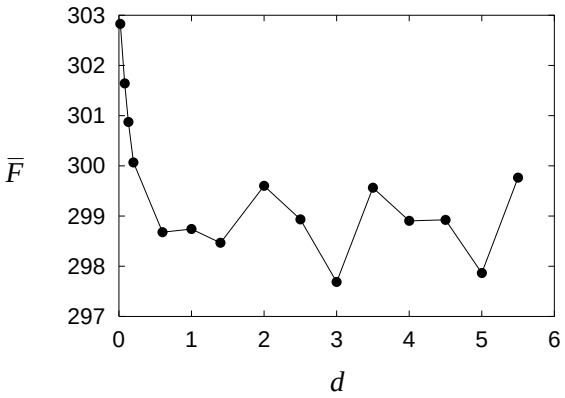

Fig. 13. The free energy $\overline{F}$ as a function of the distance d of the droplets. A repulsion for $d < 0.6$ is clearly visible.

3.4 Repulsion without defect

We return to the first geometry with two water droplets and homeotropic boundary conditions at all the surfaces. When we take either a uniform director field or randomly oriented directors as a starting configuration, our system always relaxes into the configuration sketched in Figure 12. Both water droplets are surrounded in their equatorial plane by a $-1/2$ disclination ring which compensates the point charge $+1$ each droplet carries with it [21,22]. To obtain the total point charge $+1$ of the nematic drop there has to be an additional topological defect with a point charge $+1$. In the numerically relaxed director field we find a $+1/2$ disclination ring close to the outer surface. This configuration has a higher energy than the one with the hyperbolic hedgehog. It is only metastable. Since a transition to the stable configuration needs a complete rearrangement of the director field, the energy barrier is certainly larger than $K_{33}a \approx 1000\, k_{\mathrm{B}}T$. We, therefore, expect the configuration of Figure 12 to be stable against thermal fluctuations. It would be interesting to search for it in the experiment.

We use the configuration to demonstrate that even without the hyperbolic hedgehog the two water droplets experience some repulsion when they come close to each other. In Figure 13 we plot the free energy $\overline{F}$ *versus* the distance d of the two spheres. For large d, the free energy oscillates which we attribute to numerical artifacts. For decreasing d, the free energy clearly increases, and the water droplets repel each other due to the strong deformation of the director field lines connecting the two droplets.

We thank A. Emerson, A. Kilian, A. Rüdinger, Th. Seitz, H.-R. Trebin, and S. Žumer for helpful discussions. H. S. thanks P. Poulin, T. C. Lubensky, and D. Weitz for a fruitful collaboration, which initiated the present work. J. S. gratefully acknowledges a grant from the Sonderforschungsbereich 382 of the Deutsche Forschungsgemeinschaft.

Appendix A: Method of finite elements for nematic liquid crystals in a cylindrical geometry

The major advantage of the finite element method [35] is its ability to cope with arbitrarily complex geometries. In two dimensions, *e.g.*, the integration area is subdivided into *finite elements*, which in the simplest case are triangles. In doing so, the boundaries of a complex geometry are well approximated by polygons. This is not possible within the method of finite differences, where the grid is defined by the coordinate lines. In our geometries strong director deformations occur close to the boundaries of the spheres. For a quantitative analysis it was, therefore, important to have these boundaries defined as smoothly as possible.

To determine the tilt angle field the Oseen-Zöcher-Frank free energy has to be minimized. The finite difference technique would directly address the Euler-Lagrange equation. On the other hand, the strategy of the finite element method is to start from a discretized version of the free energy and then to apply a numerical minimization scheme. In our case, the reduced free energy is written as a function $\overline{F}[\boldsymbol{\Theta}]$, where $\boldsymbol{\Theta} = (\Theta_1, \ldots, \Theta_n)$ denotes the set of tilt angles on the n vertices of the net. It can be expressed as a sum over the free energies for the individual finite elements:

$$\overline{F}[\boldsymbol{\Theta}] = \sum_{j=1}^{l} \overline{F}_j[\Theta_1^{(j)}, \Theta_2^{(j)}, \Theta_3^{(j)}],\ \Theta_1^{(j)}, \Theta_2^{(j)}, \Theta_3^{(j)} \in \boldsymbol{\Theta}. \tag{A.1}$$

The sum runs over all l triangles, and $\overline{F}_j[\Theta_1^{(j)}, \Theta_2^{(j)}, \Theta_3^{(j)}]$ is the free energy of the jth triangle as a function of the three tilt angles at the vertices of the triangle. In order to derive $\overline{F}_j[\Theta_1^{(j)}, \Theta_2^{(j)}, \Theta_3^{(j)}]$ we start from the free energy of one triangle of area $A(j)$:

$$\overline{F}_j(\Theta) = 2\pi \int_{A(j)} \mathrm{d}z\, \mathrm{d}\rho\, \rho\, \overline{f}[\Theta(\rho, z)]. \tag{A.2}$$

The quantity $\overline{f}[\Theta(\rho, z)]$ is the Oseen-Zöcher-Frank free energy density of equation (2), and an axial symmetry is assumed. Furthermore, in order to handle every finite element in the same manner, we introduce *natural* coordinates u, v:

$$\rho^{(j)}(u, v) = \rho_1^{(j)} + (\rho_2^{(j)} - \rho_1^{(j)})\, u + (\rho_3^{(j)} - \rho_1^{(j)})\, v \tag{A.3}$$

$$z^{(j)}(u, v) = z_1^{(j)} + (z_2^{(j)} - z_1^{(j)})\, u + (z_3^{(j)} - z_1^{(j)})\, v, \tag{A.4}$$

where $\rho_i^{(j)}$ and $z_i^{(j)}$ are the cylindrical coordinates of the vertices of the jth triangle ($i = 1, 2, 3$). In the new coordinates every triangle is right-angled and isosceles. The free energy now assumes the form

$$\overline{F}_j(\Theta) = 2\pi\, \Delta_j \times \int_0^1 \mathrm{d}v \int_0^{1-v} \mathrm{d}u\, \rho^{(j)}(u, v)\, \overline{f}[\Theta^{(j)}(u, v)], \tag{A.5}$$

where

$$\Delta_j = (\rho_2^{(j)} - \rho_1^{(j)})\,(z_3^{(j)} - z_1^{(j)}) - (\rho_3^{(j)} - \rho_1^{(j)})\,(z_2^{(j)} - z_1^{(j)}) \tag{A.6}$$

is the Jacobian determinant of the coordinate transformation. When the finite elements are small enough, the tilt angle field within one element is well-approximated by a linear interpolation on the area of the triangle,

$$\Theta^{(j)}(u, v) = \Theta_1^{(j)} + (\Theta_2^{(j)} - \Theta_1^{(j)})\, u + (\Theta_3^{(j)} - \Theta_1^{(j)})\, v. \tag{A.7}$$

We now insert (A.7, A.6) into (A.5). To simplify the integration over u and v we replace Θ and ρ by their average values $\rho_0^{(j)} = (\rho_1^{(j)} + \rho_2^{(j)} + \rho_3^{(j)})/3$ and $\Theta_0^{(j)} = (\Theta_1^{(j)} + \Theta_2^{(j)} + \Theta_3^{(j)})/3$. This renders the integrals trivial, yielding the free energy of the jth triangle in terms of the three tilt angles at its three vertices:

$$\overline{F}_j[\Theta_1^{(j)}, \Theta_2^{(j)}, \Theta_3^{(j)}] = \pi\, \Delta_j\, \rho_0^{(j)}\, \overline{f}[\Theta^{(j)}]. \tag{A.8}$$

The partial derivatives Θ_ρ and Θ_z necessary to compute $\overline{f}[\Theta^{(j)}]$ from equation (2) follow from

$$\Theta_\rho^{(j)} = \Theta_u^{(j)}\, u_\rho^{(j)} + \Theta_v^{(j)}\, v_\rho^{(j)}, \tag{A.9}$$

$$\Theta_z^{(j)} = \Theta_u^{(j)}\, u_z^{(j)} + \Theta_v^{(j)}\, v_z^{(j)} \tag{A.10}$$

with

$$\Theta_u^{(j)} = \Theta_2^{(j)} - \Theta_1^{(j)}, \qquad \Theta_v^{(j)} = \Theta_3^{(j)} - \Theta_1^{(j)}, \tag{A.11}$$

and

$$u_\rho^{(j)} = (z_3^{(j)} - z_1^{(j)})/\Delta_j, \tag{A.12}$$

$$v_\rho^{(j)} = -(z_2^{(j)} - z_1^{(j)})/\Delta_j, \tag{A.13}$$

$$u_z^{(j)} = -(\rho_3^{(j)} - \rho_1^{(j)})/\Delta_j, \tag{A.14}$$

$$v_z^{(j)} = (\rho_2^{(j)} - \rho_1^{(j)})/\Delta_j. \tag{A.15}$$

References

1. M. Kléman, *Points, Lines and Walls: In liquid crystals, magnetic systems, and various ordered media* (John Wiley & Sons, New York, 1983).
2. N.D. Mermin, Rev. Mod. Phys. **51**, 591 (1979).
3. H.-R. Trebin, Adv. Phys. **31**, 195 (1982).
4. M.V. Kurik, O.D. Lavrentovich, Usp. Fiz. Nauk **154**, 381 (1988) [Sov. Phys. Usp. **31**, 196 (1988)].
5. P. Chaikin, T.C. Lubensky, *Principles of Condensed Matter Physics* (Cambridge University Press, Cambridge, 1995).
6. M. Schadt, W. Helfrich, Appl. Phys. Lett. **18**, 127 (1971).
7. N. Clark, S. Lagerwall, Appl. Phys. Lett. **36**, 899 (1980).
8. J.W. Doane, N.A. Vaz, B.G. Wu, S. Žumer, Appl. Phys. Lett. **48**, 269 (1986).
9. P.S. Drzaic, *Liquid Crystal Dispersions* (World Scientific Publ., Singapore, 1995).
10. *Liquid Crystals in Complex Geometries*, edited by G.P. Crawford, S. Žumer (Taylor & Francis, London, 1996).
11. W.B. Russel, D.A. Saville, W.R. Schowalter, *Colloidal Dispersions* (Cambridge University Press, Cambridge, 1995).
12. F. Brochard, P.-G. de Gennes, J. Phys. **31**, 691 (1970).
13. J. Rault, C.R. Acad. Sci. Paris B **272**, 1275 (1971).
14. P.E. Cladis, M. Kléman, P. Piéranski, C.R. Acad. Sci. Paris B **273**, 275 (1971).
15. R. Eidenschink, W.H. de Jeu, Electron. Lett. **27**, 1195 (1991).
16. M. Kreuzer, T. Tschudi, R. Eidenschink, Mol. Cryst. Liq. Cryst. **223**, 219 (1992).
17. A. Glushchenko *et al.*, Liq. Cryst. **23**, 241 (1997).
18. P. Poulin, V.A. Raghunathan, P. Richetti, D. Roux, J. Phys. I France **4**, 1557 (1994).
19. V.A. Raghunathan, P. Richetti, D. Roux, Langmuir **12**, 3789 (1996).
20. V.A. Raghunathan *et al.*, Mol. Cryst. Liq. Cryst. **288**, 181 (1996).
21. E.M. Terentjev, Phys. Rev. E **51**, 1330 (1995).
22. O.V. Kuksenok, R.W. Ruhwandl, S.V. Shiyanovskii, E.M. Terentjev, Phys. Rev. E **54**, 5198 (1996).
23. R.W. Ruhwandl, E.M. Terentjev, Phys. Rev. E **56**, 5561 (1997).
24. S. Ramaswamy, R. Nityananda, V.A. Raghunathan, J. Prost, Mol. Cryst. Liq. Cryst. **288**, 175 (1996).
25. R.W. Ruhwandl, E.M. Terentjev, Phys. Rev. E **55**, 2958 (1997).
26. A. Borštnik, S. Žumer, Phys. Rev. E **56**, 3021 (1997).
27. P. Poulin, H. Stark, T.C. Lubensky, D.A. Weitz, Science **275**, 1770 (1997).
28. P. Poulin, D.A. Weitz, Phys. Rev. E **57**, 626 (1998).
29. R.B. Meyer, Mol. Cryst. Liq. Cryst. **16**, 355 (1972).
30. T.C. Lubensky, D. Pettey, N. Currier, H. Stark, Phys. Rev. E **57**, 610 (1998).
31. P. Poulin, V. Cabuil, D.A. Weitz, Phys. Rev. Lett. **79**, 4862 (1997).
32. N. Mermin, in *Quantum Fluids and Solids*, edited by S. Trickey, E. Adams, J. Dufty (Plenum Press, New York, 1977).
33. S. Candau, P.L. Roy, F. Debeauvais, Mol. Cryst. Liq. Cryst. **23**, 283 (1973).
34. M. Kurik, O. Lavrentovich, Pis'ma Zh. Eksp. Teor. Fiz. **35**, 65 (1982) [JETP Lett. **35**, 65 (1982)].
35. E.H. Twizell, *Computational methods for partial differential equations* (Chichester, Horwood, 1984).
36. P.-G. de Gennes, J. Prost, *The Physics of Liquid Crystals*, 2nd edn. (Clarendon Press, Oxford, 1993).
37. In nematic droplets with homeotropic anchoring a twist in the director field is usually observed (see [33]). We are currently investigating the dipole of Figure 1 and also find a twisting of the director field close to the hyperbolic hedgehog. However, for the Frank elastic constants of 5CB the distance of the defect from the surface of the water droplet differs only by 10% if the director field is not allowed to twist. We do not expect a different behavior in the geometry under consideration in this article. Performing an advanced numerical investigation of such a complex geometry, we want to concentrate, as a first step, on the principal features of the system. Therefore, we neglect twist deformations to simplify the numerics. The same simplification to catch the main behavior of nematic drops in a magnetic field was used by other authors, see, *e.g.*, [38].
38. S. Kralj, S. Žumer, Phys. Rev. A **45**, 2461 (1992); S. Komura, R.J. Atkin, M.S. Stern, D.A. Dunmur, Liq. Cryst. **23**, 193 (1997).
39. W.H. Press, S.A. Teukolsky, W.T. Vetterling, B.P. Flannery, *Numerical Recipes in Fortran: The Art of Scientific Computing* (Cambridge University Press, Cambridge, 1992).
40. L.D. Landau, E.M. Lifschitz, Statistische Physik, Teil 1, *Lehrbuch der Theoretischen Physik*, 6th edn. (Akademie-Verlag, Berlin, 1984), Vol. 5.
41. There is strictly speaking no true phase transition since our investigated system is of finite size. However, we do not expect a qualitative change in Figure 9 when the nematic drop is much larger than the enclosed water droplets ($r_3 \gg r_1, r_2$), *i.e.*, when the system reaches the limit of infinite size.